IEEE Access
Multidisciplinary ⋮ Rapid Review ⋮ Open Access Journal

Received January 20, 2019, accepted February 16, 2019, date of publication February 25, 2019, date of current version March 13, 2019.

Digital Object Identifier 10.1109/ACCESS.2019.2901366

Adaptive Backstepping Sliding Mode Control of Coaxial Octorotor Unmanned Aerial Vehicle

RASHID ALI[1], PENG YUNFENG[1], (Member, IEEE), M. TOUSEEF IQBAL[2], ROOH UL AMIN[3], M. OMER ZAHID[4], AND OMAIR IRFAN KHAN[4]

[1]School of Computer and Communication Engineering, University of Science and Technology Beijing, Beijing 100083, China
[2]Department of Electrical Engineering, University of Engineering and Technology Taxila, Taxila 47070, Pakistan
[3]School of Automation and Control, Northwestern Polytechnical University, Xi'an 710072, China
[4]School of Mechanical and Manufacturing Engineering, National University of Science and Technology, Islamabad 44000, Pakistan

Corresponding author: Rashid Ali (ist_rashid89@yahoo.com)

This work was supported by the Foundation of Guizhou Key Laboratory of Electric Power Big Data, Guizhou Institute of Technology (2003008002).

ABSTRACT In this paper, an adaptive backstepping scheme based on sliding mode control method is presented for attitude and altitude tracking control of a coaxial octorotor. The dynamical model of the coaxial octorotor is presented and according to design nature of the control scheme, the dynamical model is divided into three cascaded units: 1) under-actuated unit; 2) fully actuated unit; and 3) rotors thrust force unit. Adaptive backstepping control is then designed for all three units by means of a recursive process using sliding surfaces. The proposed scheme not only stabilizes the given system but also tracks the desired trajectory without any significant tracking error. The stability analysis of the complete system is presented using a Lyapunov stability theory. The results demonstrate the effectiveness of the proposed controller and also show that the proposed controller manages to attain good tracking performance with stabilization of octorotor.

INDEX TERMS Attitude and altitude control, adaptive backstepping scheme, coaxial octorotor, sliding mode control.

I. INTRODUCTION

During the last decade, Unmanned Aerial Vehicle (UAV) research has witnessed a paradigm shift from conventional UAV to Multirotor UAV (MUAV). The research fraternity has shown substantial interest in MUAV design and control domain. The key reasons behind this are its structural simplicity and cost effectiveness. Moreover, the enhanced reliability feature and compactness are also unavoidable. However, the aforementioned advantages cost high complexity level in controller design since MUAV(s) are highly coupled under-actuated nonlinear systems. MUAV(s) have different configurations with respect to number of rotors and shape, among which quadrotor is the most commonly used configuration. Though quadrotor usage is not a wise choice in applications that require high lifting power, high payload, and fail-safe flight in harsh environment. However, these shortcomings can be avoided by using MUAV(s) with large number of rotors such as octorotor. Octorotor encompasses all the basic advantages of quadrotor along with additional features like enhanced stability and reliability in flight missions even in case of failure of one or two rotors.

Numerous linear and nonlinear control techniques have so far been proposed for various MUAV configurations including four rotor hover vehicle [1], [4] quadrotor [5] and octorotor [6], [7] among others. However, linear controllers are based on linearized models and have not been proved efficient in inhospitable environment and for fail-safe operations. Various nonlinear controllers have been applied by the researchers for an improved MUAV control among which sliding mode control (SMC) and backstepping control proved efficient. SMC is the most easily applicable nonlinear control technique [8]. Bouabdallah and Siegwart [9] introduced SMC to address the attitude control problem of the quadrotor. The controller exhibited satisfactory simulation results but average flight performance due to chattering phenomena. Xu and Ozguner [10] modeled quadrotor as cascaded under-actuated systems and applied SMC with and without parametric uncertainties and achieved good simulation results. Bouadi and Tadjine [11] considered nonholonomic and physical constraints in system dynamics and proposed SMC for quadrotor system model. Lee *et al.* [12] provided comparison

The associate editor coordinating the review of this manuscript and approving it for publication was Xiaowei Zhao.

of adaptive SMC and feedback linearization controller (FLC). Simulation results showed that adaptive SMC exhibited efficient performance in noisy environment as compared to FLC. Luque-Vega *et al.* [13] proposed robust block second order SMC with embedment of super twisting algorithm to address the trajectory tracking control problem and compared simulation results with pioneer work of [9]. Backstepping is another well-recognized nonlinear control method, especially for control of underactuated systems. Initially Bouabdallah and Siegwart [9] applied backstepping control for quadrotor and compared its performance with SMC. The simulation results showed that backstepping control provided better performance than SMC. Madani and Benallegue [14] modified nonlinear dynamics of quadrotor and proposed backstepping control for step wise underactuated, fully actuated, and propeller system. The simulation results exhibited good stabilization and tracking performance. Das *et al.* [15] applied backstepping control on Lagrangian form dynamics of quadrotor. Huang *et al.* [16] addressed the trajectory tracking problem of quadrotor subjected to vehicle mass uncertainty using backstepping approach. Although backstepping is an efficient method for nonlinear system control and it provides fast convergence rate with an ability to handle external disturbances. Nevertheless, backstepping lacks robustness which may lead to instability resulting in failure. To address this issue several hybrid backstepping control techniques have been introduced by the researchers. For instance Colorado *et al.* [17] used hybrid backstepping control with Frenet-Serret theory to address the stabilization and attitude tracking problem of a commercial quadrotor, the Dragan Flyer. Ha *et al.* [18] proposed passivity based adaptive backstepping control of mixed type quadrotor and evaluated the performance using experimental flights.

Although coaxial octorotor has commercially been available for more than half decade in market, but literature analysis reveals that only a handful of research work has been done on octorotor control. Colorado *et al.* [7] proposed dynamical model of coaxial octorotor and implemented PID controller for attitude tracking problem. The simulation and experimental results were not quite satisfactory as the octorotor was fixed on a ball joint to allow only rotational motion. Peng *et al.* [6] claimed to develop the first dynamical model of the coaxial octorotor. They proposed robust backstepping sliding mode controller (BSMC) and used radial basis function network (RBFN) to estimate the system uncertainties. However, only attitude tracking problem was addressed and proposed BSMC controllers were designed separately for roll, pitch and yaw channels instead of a single BSMC for attitude and altitude control of octorotor. Peng *et al.* [19] also proposed variable structure and variable coefficient PID (VSVCPID) anti-windup control for yaw channel to prevent actuator saturation and verified the proposed algorithm with numerical simulations and experiments. Saied *et al.* [20] presented fault tolerant control (FTC) control strategy in case of rotor failure in coaxial octorotor. The FTC comprised of a nonlinear observer and an inference model to detect and isolate the faulty rotor, and a recovery algorithm to compensate the loss of faulty rotor to maintain a stable flight. Saied *et al.* [21] proposed fault diagnosis strategy based on second order sliding mode observer (SOSMO) and modified super-twisting algorithm. The proposed strategy was tested using simulations and experiment. Saied *et al.* [22] extended the previous work and presented FTC strategy for multiple rotors failure based on offline control mixing and nonlinear sliding mode observer. The proposed solution was computationally efficient and fast as compared to the previous one. The proposed strategy was tested for octorotor up to four rotor failures.

In this work adaptive backstepping sliding mode control (ABSMC) is introduced to address the attitude and altitude tracking problem of the coaxial octorotor. First, dynamic model of octorotor is developed using Newton's and Euler's equations. Afterwards, the dynamical model is modified and is divided into three units i.e. fully actuated unit, under actuated unit and input force (thrust) unit. A backstepping controller based on SMC is designed using Lyapunov candidate functions by recursion process for overall system. The stability of each unit and overall system stability is guaranteed using Lyapunov stability theory. To the best of authors' knowledge, the proposed controller is the first nonlinear controller to address the attitude and altitude tracking problem of the coaxial octorotor. The controller is tested on coaxial octorotor and simulation results are provided to demonstrate the effectiveness of the proposed controller.

The rest of the paper is structured as follows. Dynamic model of the coaxial octorotor is presented in Section II. Section III provides insight of adaptive backstepping sliding mode controller design. Simulation results and discussion is provided in Section IV. Finally, concluding remarks are presented in Section V.

II. DYNAMIC MODEL OF COAXIAL OCTOROTOR

The octorotor comprised of eight rotors, organized as four pairs of coaxial rotors attached at the ends of a cross frame structure, as shown in Figure 1. The rotor speed is ω_i and thrust of each rotor in the direction of the rotor axis is T_i where $i = 1, 2, \ldots, 8$. Each rotor in the coaxial pair rotates in the opposite direction. Moreover, the adjacent rotors also rotate in opposite direction. Therefore rotors 1, 4, 5, 8 rotate in clockwise direction and rotors 2, 3, 6, 7 rotate in counter clockwise direction. The variation in speed of the front right pair of rotors (3, 4) as compared to the back left pair of rotors (7, 8) causes the octorotor to move around the pitch axis. The roll movement is achieved by speed difference of front left rotors (1, 2) with respect to back right rotors (5, 6). The Yaw movement is obtained by speeding up or down the clockwise rotors (1, 4, 5, 8) with the same speed but in opposite direction for the counter clockwise rotors (2, 3, 6, 7). The altitude motion is obtained when speed of all of the rotors is varied together with same magnitude. The translation motion is achieved by combination of pitch and roll movement.

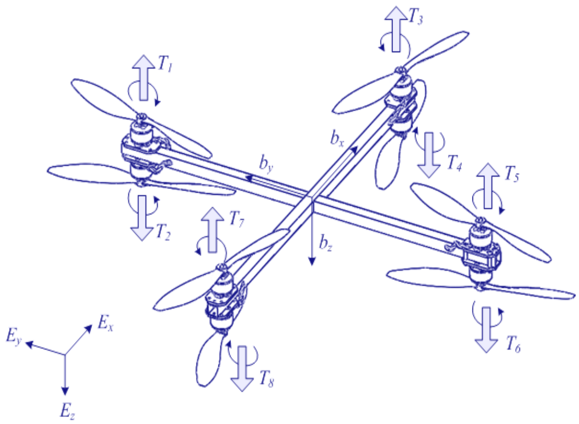

FIGURE 1. Configuration of coaxial octorotor.

Two frames of references are used for modeling of octorotor; earth fixed inertial frame defined as (E_x, E_y, E_z) and body fixed frame defined as (b_x, b_y, b_z) fixed at the center of the mass of the octorotor. The absolute positions and the attitude angles of octorotor in the inertial frame are defined as $\boldsymbol{\xi} = [x\ y\ z]^T$ and $\boldsymbol{\eta} = [\phi\ \theta\ \psi]^T$ respectively where ϕ is roll angle, θ is pitch angle, and ψ is yaw angle. The linear and angular velocities in the body frame are defined as $\boldsymbol{V}_B = \left[v_x\ v_y\ v_z\right]^T$ and $\vartheta_B = [p\ q\ r]^T$ respectively. The relati-onship between attitude angles and angular velocities is given as

$$\vartheta_B = \boldsymbol{R}_r \dot{\boldsymbol{\eta}} \tag{1}$$

where R_r is transformation matrix and given as

$$\boldsymbol{R}_r = \begin{bmatrix} 1 & 0 & -\sin\theta \\ 0 & \cos\phi & \sin\phi\cos\theta \\ 0 & -\sin\phi & \cos\phi\cos\theta \end{bmatrix} \tag{2}$$

The rotational dynamics of octorotor are derived using Euler's equation for rigid body dynamic, which is given as

$$\boldsymbol{J}\dot{\vartheta}_B + \vartheta_B \times (\boldsymbol{J}\vartheta_B) = \boldsymbol{\Gamma} + T_a \tag{3}$$

where J is the inertia matrix, T_a is aerodynamic friction torqueand Γ is an external torques vector given as:

$$\boldsymbol{J} = \begin{bmatrix} J_x x & 0 & 0 \\ 0 & J_y y & 0 \\ 0 & 0 & J_z z \end{bmatrix} \tag{4}$$

$$T_a = K_r \vartheta_B = K_r \boldsymbol{R}_r \dot{\boldsymbol{\eta}} \tag{5}$$

$$\Gamma = \begin{bmatrix} \tau_\phi \\ \tau_\theta \\ \tau_\psi \end{bmatrix} = \begin{bmatrix} l_{cg}\,(T_5 + T_6 - T_1 - T_2) \\ l_{cg}\,(T_3 + T_4 - T_7 - T_8) \\ Q_1 - Q_2 - Q_3 + Q_4 + Q_5 - Q_6 - Q_7 + Q_8 \end{bmatrix} \tag{6}$$

where l_{cg} is the distance between rotor and center of gravity, K_r is the aerodynamic coefficient, $T_i = k\omega_i^2$ is the rotors' thrust, $Q_i = b\omega_i^2$ is the aerodynamic drag, k is the lift constant and b is the drag constant.

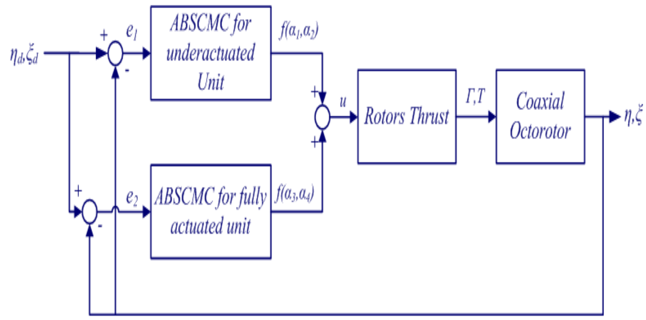

FIGURE 2. Block diagram of ABSMC scheme for coaxial octorotor.

In order to determine rotational equations of motion in the body frame, equation (3) can be rewritten as

$$\dot{\vartheta}_B = \boldsymbol{J}^{-1}(\boldsymbol{\Gamma} + T_a - \boldsymbol{R}_r\dot{\boldsymbol{\eta}} \times (\boldsymbol{J}\boldsymbol{R}_r\dot{\boldsymbol{\eta}})) \tag{7}$$

The linear motion of the octorotor in inertial frame is given by Newton's second law

$$\boldsymbol{F} = m\boldsymbol{G} - \boldsymbol{F}_t - \boldsymbol{F}_a \tag{8}$$

where thrust force, $\boldsymbol{F}_t$ and aerodynamic force, $\boldsymbol{F}_a$ are given as

$$\begin{aligned} \boldsymbol{F}_t &= \boldsymbol{R}_t\boldsymbol{T}_B \\ \boldsymbol{F}_a &= K_t\boldsymbol{V}_B = K_t\boldsymbol{R}_t^T\dot{\boldsymbol{\xi}} \end{aligned} \tag{9}$$

Equation (8) can be written as

$$m\ddot{\boldsymbol{\xi}} = m\boldsymbol{G} - \boldsymbol{R}_t\boldsymbol{T}_B - K_t\boldsymbol{R}_t^T\boldsymbol{\xi} \tag{10}$$

where $\boldsymbol{R}_t$ is rotation matrix from the body frame to the inertial frame, $\boldsymbol{T}_B$ is total body thrust, K_t is the aerodynamic friction coefficient, and G is gravity vector and are given as (11), as shown at the top of the next page.

The overall dynamical model of octorotor using equations (1), (7) and (10) can be written as:

$$\begin{aligned} \ddot{\boldsymbol{\xi}} &= \boldsymbol{G} - \frac{1}{m}\boldsymbol{R}_t\boldsymbol{T}_B - \frac{1}{m}K_t\boldsymbol{R}_t^T\boldsymbol{\xi} \\ \ddot{\boldsymbol{\eta}} &= (\boldsymbol{R}_r\boldsymbol{J})^{-1}\,(\boldsymbol{\Gamma} + T_a - \boldsymbol{R}_r\dot{\boldsymbol{\eta}} \times (\boldsymbol{J}\boldsymbol{R}_r\dot{\boldsymbol{\eta}})) \end{aligned} \tag{12}$$

III. ADAPTIVE BACKSTEPPING SLIDING MODE CONTROL DESIGN

In this section, adaptive backstepping control approach based on SMC is presented to address the attitude and altitude control problem of the coaxial octorotor. The control diagram is shown in Figure 2. The adaptive backstepping is a recursive process in which a system is split into cascaded systems or nested loops and then step wise adaptive control design is applied. The design approach is to start stabilization from the simple cascaded system or the inner loopusing Lyapunov stability theorem and then ''back step'' to the outer loops or other cascaded systems until the control input is obtained.

To design the ABSMC scheme, the dynamical model of the coaxial octorotor is divided into three units:

$$\boldsymbol{R}_t = \begin{bmatrix} \cos\theta\cos\psi & \sin\phi\sin\theta\cos\psi - \cos\phi\sin\psi & \cos\phi\sin\theta\cos\psi + \sin\phi\sin\psi \\ \cos\theta\sin\psi & \sin\phi\sin\theta\sin\psi + \cos\phi\cos\psi & \cos\phi\sin\theta\sin\psi - \sin\phi\cos\psi \\ -\sin\theta & \sin\phi\cos\theta & \cos\phi\cos\theta \end{bmatrix}$$

$$\boldsymbol{T}_B = \begin{bmatrix} 0 \\ 0 \\ T \end{bmatrix}, \quad \boldsymbol{G} = \begin{bmatrix} 0 \\ 0 \\ g \end{bmatrix}, \quad T = \sum_{i=1}^{8} T_i = k\sum_{i=1}^{8}\omega_i^2 \tag{11}$$

(i) Under actuated unit (with roll, pitch, and x, y positions as state vectors).

(ii) Fully actuated unit (with yaw and z position as state vectors).

(iii) Rotor force (thrust) unit.

The system states for the above mentioned units are defined as

$$x_1 = \begin{bmatrix} x \\ y \\ \phi \\ \theta \end{bmatrix}, \quad x_2 = \begin{bmatrix} \dot{x} \\ \dot{y} \\ \dot{\phi} \\ \dot{\theta} \end{bmatrix}, \quad x_3 = \begin{bmatrix} z \\ \psi \end{bmatrix}, \quad x_4 = \begin{bmatrix} \dot{z} \\ \dot{\psi} \end{bmatrix},$$
$$x_5 = \begin{bmatrix} T_1 & T_2 & T_3 & T_4 & T_5 & T_6 & T_7 & T_8 \end{bmatrix}^T \tag{13}$$

The dynamics of the octorotor defined in equation (12) are now redefined according to the states defined in equation (13) as follows:

$$\begin{aligned} \dot{x}_1 &= x_2 \\ \dot{x}_2 &= f_1(x_1, x_2, x_3, x_4, x_5) + g_1(x_1)w_1(x_5) \\ \dot{x}_3 &= x_4 \\ \dot{x}_4 &= f_2(x_1, x_2, x_3, x_4, x_5) + g_2(x_1)w_2(x_5) \\ \dot{x}_5 &= u \end{aligned} \tag{14}$$

where the matrices g_1, w_1, g_2, and w_2 are defined as (15), as shown at the top of the next page.

The vectors f_1 and f_2 are defined as

$$f_1 = \begin{bmatrix} f_x \\ f_y \\ f_\phi \\ f_\theta \end{bmatrix}, \quad f_2 = \begin{bmatrix} f_z \\ f_\psi \end{bmatrix} \tag{16}$$

where

$$\begin{bmatrix} f_x \\ f_y \\ f_z \end{bmatrix} = \boldsymbol{G} - \frac{1}{m}K_t\boldsymbol{R}_t^T\dot{\boldsymbol{\xi}}$$
$$\begin{bmatrix} f_\phi \\ f_\theta \\ f_\psi \end{bmatrix} = (\boldsymbol{R}_r\boldsymbol{J})^{-1}\left(K_r\boldsymbol{R}_r\dot{\boldsymbol{\eta}} - \boldsymbol{R}_r\dot{\boldsymbol{\eta}} \times (\boldsymbol{J}\boldsymbol{R}_r\dot{\boldsymbol{\eta}})\right)$$
$$+ \frac{\tau_\phi}{J_y}\begin{bmatrix} \sin\phi\tan\theta \\ \cos\phi \\ \dfrac{\sin\phi}{\cos\theta} \end{bmatrix} \tag{17}$$

The objective is to design control of coaxial octorotor such that the system outputs (ξ, η) track the desired trajectory and error converges to zero asymptotically. The control design process is divided into following five steps.

A. STEP 1

The tracking error vector for the under actuated unit is defined as following:

$$e_1 = x_{1d} - x_1 \tag{18}$$

The first Lyapunov candidate function is selected as

$$V_1 = \frac{1}{2}e_1^Te_1 \tag{19}$$

The derivative of V_1 is given as

$$\dot{V}_1 = e_1^T\dot{e}_1 = e_1^T(\dot{x}_{1d} - \dot{x}_1) \tag{20}$$

The stabilization of e_1 requires $\dot{V}_1 < 0$, therefore the first virtual control input α_1 is introduced as

$$\begin{aligned} \alpha_1 &= \dot{x}_1 \\ &= A_1e_1 + \dot{x}_{1d} \end{aligned} \tag{21}$$

where $A_1 \in R^{4\times4}$ is a positive definite gain matrix. Substituting α_1 from equation (21), the equation (20) becomes

$$\dot{V}_1 = -e_1^TA_1e_1 < 0 \tag{22}$$

Thus e_1 is guaranteed to converge to zero asymptotically.

B. STEP 2

In this step, the under actuated unit is modified into following virtual system

$$\dot{x}_2 = f_1(x_1, x_2, x_3, x_4, x_5) + g_1(x_1)\alpha_2 \tag{23}$$

where α_2 is the second virtual control input. The sliding surface for this virtual system is defined as

$$\begin{aligned} s_1 &= \alpha_1 - x_2 \\ &= A_1e_1 + \dot{x}_{1d} - \dot{x}_1 \\ &= A_1e_1 + \dot{e}_1 \end{aligned} \tag{24}$$

where $s_1 = diag[s_{11}, s_{12}, s_{13}, s_{14}]$

The Lyapunov function for this step is considered as

$$V_2 = \frac{1}{2}\left(e_1^Te_1 + s_1^Ts_1\right) \tag{25}$$

The derivative of V_2 is given as

$$\begin{aligned} \dot{V}_2 &= e_1^T\dot{e}_1 + s_1^T\dot{s}_1 \\ &= -e_1^TA_1e_1 + s_1^T(\dot{\alpha}_1 - \dot{x}_2) \\ &= -e_1^TA_1e_1 + s_1^T(\dot{\alpha}_1 - f_1 - g_1\alpha_2) \end{aligned} \tag{26}$$

$$g_1 = \begin{bmatrix} \frac{1}{m}\sin\phi\sin\psi & -\frac{1}{m}\cos\phi\cos\psi\sin\theta & 0 & 0 \\ \frac{1}{m}\cos\psi\sin\phi & -\frac{1}{m}\cos\phi\sin\psi\sin\theta & 0 & 0 \\ 0 & 0 & \frac{1}{J_x} & \frac{1}{J_z}\cos\theta\tan\theta \\ 0 & 0 & 0 & \frac{1}{J_z}\sin\phi \end{bmatrix},$$

$$w_1 = \begin{bmatrix} \sum_{i=1}^{8} T \\ \sum_{i=1}^{8} T \\ \tau_\theta \\ \tau_\psi \end{bmatrix}$$

$$g_2 = \begin{bmatrix} \frac{1}{m}\cos\phi\cos\theta & 0 \\ 0 & \frac{1}{J_z}\frac{\cos\phi}{\cos\theta} \end{bmatrix}, \quad w_2 = \begin{bmatrix} \sum_{i=1}^{8} T_i \\ \tau_\psi \end{bmatrix} \tag{15}$$

The sliding surface can be stabilized by introducing following virtual control input

$$\alpha_2 = g_1^{-1}\left(\dot{\alpha}_1 - f_1 + \gamma_1 s_1 + \Lambda_1 sgn(s_1)\right) \tag{27}$$

where γ_1 is an adaptive gain matrix and Λ_1 is a positive definite gain matrix. The substitution of virtual control input α_2 into equation (26) results

$$\begin{aligned} \dot{V}_2 &= -e_1^T A_1 e_1 - s_1^T \gamma_1 s_1 - s_1^T \Lambda_1 sgn(s_1) \\ &= \dot{V}_1 - s_1^T \gamma_1 s_1 - s_1^T \Lambda_1 sgn(s_1) \leq 0 \end{aligned} \tag{28}$$

Thus e_1 and s_1 are guaranteed to converge to zero asymptotically and the under actuated unit is asymptotically stable.

C. STEP 3

For fully actuated unit, the tracking error is defined as

$$e_2 = x_{3d} - x_3 \tag{29}$$

The Lyapunov function for this step is considered as

$$V_3 = \frac{1}{2} e_2^T e_2 \tag{30}$$

The derivative of V_3 is given as

$$\dot{V}_3 = e_2^T \dot{e}_2 = e_2^T\left(\dot{x}_{3d} - \dot{x}_3\right) \tag{31}$$

The stabilization of e_2 requires $\dot{V}_3 < 0$, therefore the third virtual control input α_3 is considered as

$$\begin{aligned} \alpha_3 &= \dot{x}_3 \\ &= A_2 e_2 + \dot{x}_{3d} \end{aligned} \tag{32}$$

where $A_2 \in R^{2\times 2}$ is a positive definite gain matrix. Substituting α_3 from equation (32), the equation (31) becomes

$$\dot{V}_3 = -e_2^T A_2 e_2 < 0 \tag{33}$$

Thus e_2 is guaranteed to converge to zero asymptotically.

D. STEP 4

In this step, the fully actuated unit is modified to following virtual system

$$\dot{x}_4 = f_2(x_1, x_2, x_3, x_4, x_5) + g_2(x_1)\alpha_4 \tag{34}$$

where α_4 is the fourth virtual control input. The sliding surface for this virtual system is defined as

$$\begin{aligned} s_2 &= \alpha_3 - x_4 \\ &= A_2 e_2 + \dot{x}_{3d} - \dot{x}_3 \\ &= A_2 e_2 + \dot{e}_2 \end{aligned} \tag{35}$$

where $s_2 = diag\,[s_{21}, s_{22}]$

The Lyapunov function for this step is considered as

$$V_4 = \frac{1}{2}\left(e_2^T e_2 + s_2^T s_2\right) \tag{36}$$

The derivative of V_4 is given as

$$\begin{aligned} \dot{V}_4 &= e_2^T \dot{e}_2 + s_2^T \dot{s}_2 \\ &= -e_2^T A_2 e_2 + s_2^T\left(\dot{\alpha}_3 - \dot{x}_4\right) \\ &= -e_2^T A_1 e_2 + s_2^T\left(\dot{\alpha}_3 - f_2 - g_2\alpha_4\right) \end{aligned} \tag{37}$$

The sliding surface vector can be stabilized by introducing following virtual control input

$$\alpha_4 = g_2^{-1}\left(\dot{\alpha}_3 - f_2 + \gamma_2 s_2 + \Lambda_2 sgn(s_2)\right) \tag{38}$$

where γ_2 is an adaptive gain matrix and Λ_2 is a positive definite gain matrix. The substitution of virtual control input α_4 into equation (38) results

$$\begin{aligned} \dot{V}_4 &= -e_2^T A_2 e_2 - s_2^T \gamma_2 s_2 - s_2^T \Lambda_2 sgn(s_2) \\ &= \dot{V}_3 - s_2^T \gamma_2 s_2 - s_2^T \Lambda_2 sgn(s_2) \leq 0 \end{aligned} \tag{39}$$

Thus e_2 and s_2 are guaranteed to converge to zero asymptotically and the fully actuated unit is asymptotically stable.

Remark 1: The Levenberg-Marquardt algorithm (LMA) is used to update adaptive gains γ_1 and γ_2. The cost functions according to the sliding surface are defined as

$$E_1 = \frac{1}{2}\sum_{m=1}^{q}(\alpha_1 - x_2)^2 = \frac{1}{2}\sum_{m=1}^{q}\zeta_{m1}^2$$
$$E_2 = \frac{1}{2}\sum_{m=1}^{q}(\alpha_3 - x_4)^2 = \frac{1}{2}\sum_{m=1}^{q}\zeta_{m2}^2$$

The LMA is defined as following to update the adaptive gain

$$\left[J_a^T(\gamma_i)J_a(\gamma_i) + \lambda_i I_a\right]\Delta\gamma_i = J_a^T(\gamma_i)\zeta_{mi}(\gamma_i)$$
$$\Delta\gamma_i = -\left[J_a^T(\gamma_i)J_a(\gamma_i) + \lambda_i I_a\right]^{-1} \times \nabla E_i(\gamma_i)$$

where γ_i is adaptive gain matrix, $\zeta_{mi}(\gamma_i)$ is the error matrix, $J_a^T(\gamma_i)$ is the Jacobian matrix of $\zeta_{mi}(\gamma_i)$, I_a is identity matrix, λ is variable parameter and $\nabla E_i(\gamma_i) = J_a^T(\gamma_i)\zeta_{mi}(\gamma_i)$. The adaptive gain matrix continues to update until the cost function E_i is optimized.

E. STEP 5

The tracking error for external force thrust is defined as

$$e_3 = \begin{bmatrix}\alpha_2 - w_1\\ \alpha_4 - w_2\end{bmatrix} = \begin{bmatrix} g_1^{-1}(\dot{\alpha}_1 - f_1 + \gamma_1 s_1 + \Lambda_1 sgn(s_1)) - w_1 \\ g_2^{-1}(\dot{\alpha}_3 - f_2 + \gamma_2 s_2 + \Lambda_2 sgn(s_2)) - w_2\end{bmatrix} = \begin{bmatrix} g_1^{-1}(\dot{\alpha}_1 - f_1 - g_1 w_1 + \gamma_1 s_1 + \Lambda_1 sgn(s_1)) \\ g_2^{-1}(\dot{\alpha}_3 - f_2 - g_2 w_2 + \gamma_2 s_2 + \Lambda_2 sgn(s_2))\end{bmatrix} \quad (40)$$

Using expressions for $\dot{s}_1$ and $\dot{s}_2$ defined in equations (26) and (37), the following can be derived from equation (40)

$$\dot{s}_1 = \dot{\alpha}_1 - f_1 - g_1 w_1$$
$$\dot{s}_2 = \dot{\alpha}_3 - f_2 - g_2 w_2 \quad (41)$$

Now the equation (40) can be written as

$$e_3 = \begin{bmatrix} g_1^{-1}(\dot{s}_1 + \gamma_1 s_1 + \Lambda_1 sgn(s_1)) \\ g_2^{-1}(\dot{s}_2 + \gamma_2 s_2 + \Lambda_2 sgn(s_2))\end{bmatrix} \quad (42)$$

The Lyapunov function for the complete dynamical model is given as

$$V_5 = \frac{1}{2}\sum_{i=1}^{3}\left(e_i^T e_i\right) + \frac{1}{2}\sum_{i=1}^{2}\left(s_i^T s_i\right)$$
$$\dot{V}_5 = \sum_{i=1}^{3}\left(e_i^T \dot{e}_i\right) + \sum_{i=1}^{2}\left(s_i^T \dot{s}_i\right)$$
$$= -e_1^T A_1 e_1 - e_2^T A_2 e_2 + e_3^T\left(\begin{bmatrix}\dot{\alpha}_2 - \dot{w}_1\\ \dot{\alpha}_4 - \dot{w}_2\end{bmatrix}\right) - e_1^T A_1 e_1 - s_1^T\gamma_1 s_1 - s_1^T\Lambda_1 sgn(s_1) - e_2^T A_2 e_2 - s_2^T\gamma_2 s_2 - s_2^T\Lambda_2 sgn(s_2)$$
$$= -\sum_{i=1}^{2}\left(2e_i^T A_i e_i - s_i^T\gamma_i s_i - s_i^T\Lambda_i sgn(s_i)\right) + e_3^T\left(\begin{bmatrix}\dot{\alpha}_2\\ \dot{\alpha}_4\end{bmatrix} - \begin{bmatrix}\dot{w}_1\\ \dot{w}_2\end{bmatrix}\right)$$
$$= -\sum_{i=1}^{2}\left(2e_i^T A_i e_i - s_i^T\gamma_i s_i - s_i^T\Lambda_i sgn(s_i)\right) + e_3^T\left(\begin{bmatrix}\dot{\alpha}_2\\ \dot{\alpha}_4\end{bmatrix} - \begin{bmatrix}J_1\\ J_2\end{bmatrix}u\right) \quad (43)$$

where J_1 and J_2 are Jacobian matrices of w_1 and w_2 and are given as

$$J_1 = \frac{\partial w_1}{\partial u} = \begin{bmatrix} 1 & 1 & 1 & 1 & 1 & 1 & 1 & 1\\ 1 & 1 & 1 & 1 & 1 & 1 & 1 & 1\\ 0 & 0 & 1 & 1 & 0 & 0 & -1 & -1\\ b & -b & -b & b & b & -b & -b & b\end{bmatrix}$$
$$J_2 = \frac{\partial w_2}{\partial u} = \begin{bmatrix} 1 & 1 & 1 & 1 & 1 & 1 & 1 & 1\\ b & -b & -b & b & b & -b & -b & b\end{bmatrix} \quad (44)$$

The complete model can be stabilized by introducing the following control law

$$u = \begin{bmatrix}J_1\\ J_2\end{bmatrix}^{-1}\left(\begin{bmatrix}\dot{\alpha}_2\\ \dot{\alpha}_4\end{bmatrix} + A_3 e_3\right) \quad (45)$$

where $A_3 \in R^{6\times 8}$ is positive definite gain matrix. Substituting the control law in equation (43) results in

$$\dot{V}_5 = -\sum_{i=1}^{2}\left(e_i^T A_i e_i - s_i^T\gamma_i s_i - s_i^T\Lambda_i sgn(s_i)\right) - \sum_{i=1}^{3}\left(e_i^T A_i e_i\right)$$
$$= \sum_{i=1}^{4}\dot{V}_i - e_3^T A_3 e_3 \le 0 \quad (46)$$

Hence it showed that the proposed adaptive backstepping control based on SMC not only tracks the desired reference trajectory but also guarantees the asymptotic stability.

IV. RESULTS

In this section performance of the proposed ABSMC controller is evaluated on simulation model of indigenously built coaxial octorotor. The parameters of coaxial octorotor are given in Table 1.

Two cases of simulations are presented in this work to demonstrate the performance of the proposed control scheme. In the first case, step response of the coaxial octorotor is obtained and in the second case trajectory tracking performance of coaxial octorotor is studied for a given reference trajectory. The following values have been selected for controller parameters.

$$A_1 = \text{diag}\begin{bmatrix}2 & 2 & 2 & 2\end{bmatrix}, \quad A_2 = \text{diag}\begin{bmatrix}2 & 2\end{bmatrix}$$

TABLE 1. Parameters of coaxial octorotor.

Parameter	Description	Value	Unit
m	Mass	3.2	Kg
l_{cg}	Distance between centre of gravity and each rotor	0.2	m
J_{xx}	Moment of inertia about the x axis	0.02512	Kg.m2
J_{yy}	Moment of inertia about the y axis	0.02512	Kg.m2
J_{zz}	Moment of inertia about the z axis	0.04265	Kg.m2
K_r	Aerodynamic force coefficient	0.001	Nm.s/rad
K_t	Aerodynamic friction coefficient	0.02	N.s/m

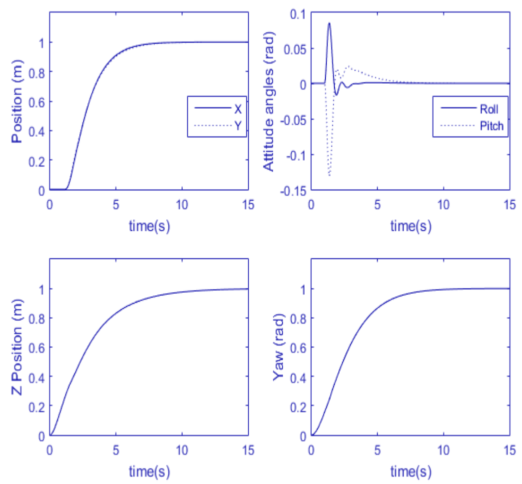

FIGURE 3. Step response of the coaxial octorotor.

$$
\begin{aligned}
A_3 &= \left[\operatorname{diag}\left[2 \quad 2 \quad 2 \quad 2 \quad 2 \quad 2\right] 0_{6\times 2}\right] \\
\Lambda_1 &= \operatorname{diag}\left[1 \quad 1 \quad 1 \quad 1\right], \quad \Lambda_2 = \operatorname{diag}\left[1 \quad 1\right] \\
\gamma_1 &= \operatorname{diag}\left[0.5 \quad 0.5 \quad 0.5 \quad 0.5\right] \\
\gamma_2 &= \operatorname{diag}\left[0.5 \quad 0.5\right], \quad \lambda = 0.1
\end{aligned} \tag{47}
$$

A. CASE 1

In the first case, a step input of amplitude 1 meter is selected for x, y, and z positions and 1radian is selected for yaw channel. The step response of the coaxial octorotor is shown in Figure 3 and error response is shown in Figure 4, respectively. It is clear that systems' outputs reached to the desired levels with smooth transient and steady state responses. A time delay can be observed in x and y position which is because the octorotor needs to attain some height (in z-axis) before it can follow the other reference trajectories. Roll and pitch responses are the result of combined x and y motion which were also smooth and became zero after octorotor reached to the desired position. The rotors' thrust is shown in Figure 5. It is clear that the desired control inputs are practically acceptable and can be provided in an experimental system.

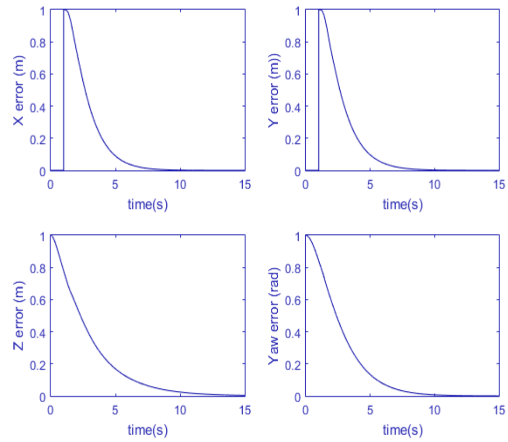

FIGURE 4. Error response of the step input.

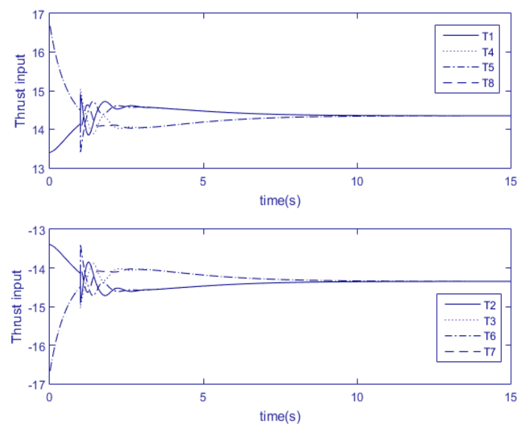

FIGURE 5. Thrust inputs.

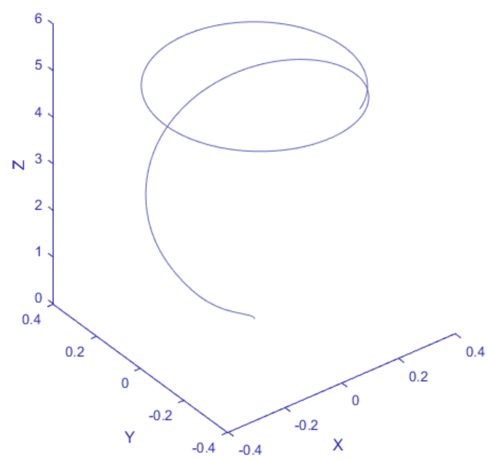

FIGURE 6. 3D plot of the octorotor output trajectory.

B. CASE 2

In the second case, sinusoidal inputs of 0.5 meter are selected for x and y positions with phase difference of 90° (i.e. circular motion in xy direction with radius 0.25 meter), reference

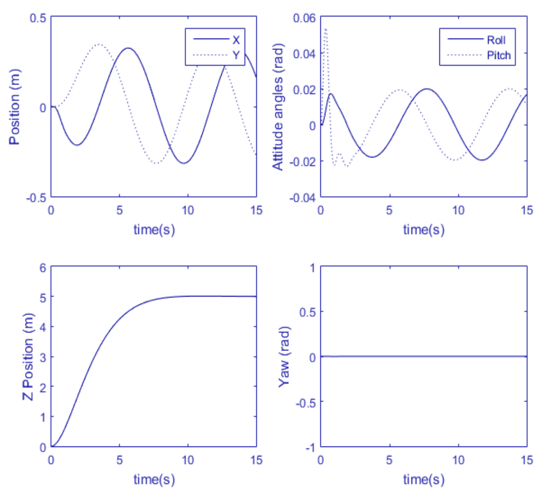

FIGURE 7. Tracking response to the reference trajectory.

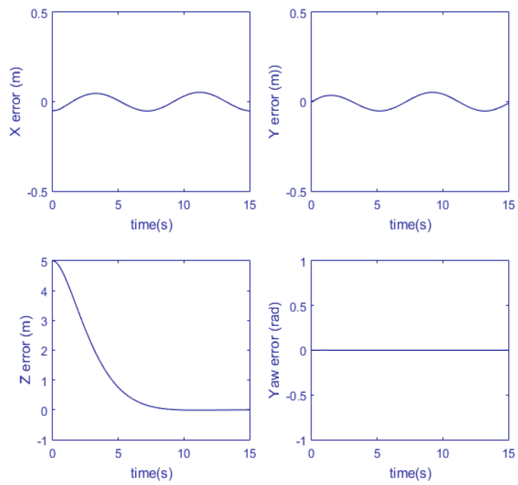

FIGURE 8. Tracking error response.

altitude (z-axis) is selected as 5 meters, and no reference input is selected for the yaw channel. Output response of the coaxial octorotor in 3D is shown in Figure 6. It is clear that octorotor attains some altitude before it starts to track the remaining desired input trajectories. The tracking response and error responses are shown in Figure 7 and 8, respectively. The responses clearly state that the proposed controller not only stabilizes the octorotor but also tracks the desired trajectory with error in an acceptable range. The time delay in altitude is the practical time required by octorotor to reach 5meters height. The zero error in yaw channel shows that the proposed control scheme manages to avoid the undesired yaw motion which is the required feature in many surveillance applications. The resulting roll and pitch motions are also smooth and are within practical limits. The rotors thrust inputs are shown in Figure 9. It can be seen that the calculated thrust inputs are within limits and are practically realizable.

The results exhibit that the proposed ABSMC scheme achieves good stabilizing and tracking performance for

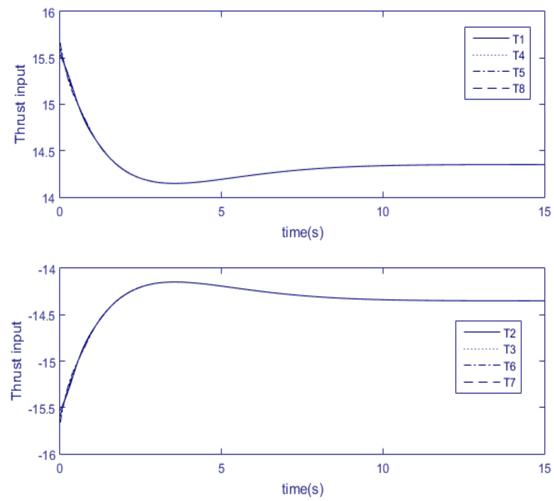

FIGURE 9. Thrust inputs.

desired reference trajectory and produces the realizable control inputs.

V. CONCLUSION

In this paper, sliding mode control based adaptive backstepping design is proposed for attitude and altitude tracking control of coaxial octorotor. First, the dynamical model of the coaxial octorotor is presented. Then, the dynamical model is divided into three units i.e. under actuated, fully actuated, rotors thrust force units to design recursive adaptive backstepping scheme based on sliding mode control. The Lyapunov stability theorem is used to provide the stability analysis of the complete system. The LMA is used to update adaptive gains used in the proposed controller. Simulation results verify that the proposed control scheme not only stabilizes the octorotor but also tracks the desired reference trajectory without observable error. Future work involves estimation of unmodeled dynamics and augmentation of wind observer for improved flight stability in harsh environments.

REFERENCES

[1] R. U. Amin, L. Aijun, L. Hongshi, and L. Jiaxing, "An adaptive sliding mode control based on radial basis function network for attitude tracking control of four rotor hover system," in *Proc. IEEE Chin. Guid., Navigat. Control Conf.*, Aug. 2016, pp. 580–585.
[2] R. U. Amin and L. Aijun, "Modelling and robust attitude trajectory tracking control of 3-DOF four rotor Hover vehicle," *Aircr. Eng. Aerosp. Technol.*, vol. 89, no. 1, pp. 87–98, 2017.
[3] R. U. Amin and L. Aijun, "Design of mixed sensitivity H_∞ control for four-rotor hover vehicle," *Int. J. Autom. Control*, vol. 11, no. 1, pp. 89–103, 2016.
[4] R. U. Amin, L. Aijun, M. U. Khan, S. Shamshirband, and A. Kamsin, "An adaptive trajectory tracking control of four rotor hover vehicle using extended normalized radial basis function network," *Mech. Syst. Signal Process.*, vol. 83, pp. 53–74, Jan. 2016.
[5] R. U. Amin, L. Aijun, and S. Shamshirband, "A review of quadrotor UAV: Control methodologies and performance evaluation," *Int. J. Autom. Control*, vol. 10, no. 2, pp. 87–103, 2016.
[6] C. Peng, Y. Bai, X. Gong, Q. Gao, C. Zhao, and Y. Tian, "Modeling and robust backstepping sliding mode control with Adaptive RBFNN for a novel coaxial eight-rotor UAV," *IEEE/CAA J. Automatica Sinica*, vol. 2, no. 1, pp. 56–64, Jan. 2015.

[7] S. J. Haddadi, P. Zarafshan, and F. J. Niroumand, "Dynamics modelling and implementation of an attitude control on an Octorotor," in *Proc. IEEE 28th Can. Conf. Elect. Comput. Eng.*, May 2015, pp. 722–727.
[8] A. Utkin, J. Guldner, and J. Shi, *Sliding Mode Control in Electro-Mechanical Systems*. London, U.K.: Taylor & Francis Ltd, 2009.
[9] S. Bouabdallah and R. Siegwart, "Backstepping and sliding-mode techniques applied to an indoor micro quadrotor," in *Proc. IEEE Int. Conf. Robot. Automat.*, Apr. 2005, pp. 2247–2252.
[10] R. Xu and U. Ozguner, "Sliding mode control of a quadrotor helicopter," in *Proc. 45th IEEE Conf. Decis. Control*, Dec. 2006, pp. 4957–4962.
[11] H. Bouadi and M. Tadjine, "Nonlinear observer design and sliding mode control of four rotors helicopter," *World Acad. Sci., Eng. Technol.*, vol. 1, no. 7, pp. 329–334 2007.
[12] D. Lee, H. J. Kim, and S. Sastry, "Feedback linearization vs. Adaptive sliding mode control for a quadrotor helicopter," *Int. J. Control, Autom., Syst.*, vol. 7, no. 3, pp. 419–428, 2009.
[13] L. Luque-Vega, B. Castillo-Toledo, and A. G. Loukianov, "Robust block second order sliding mode control for a quadrotor," *J. Franklin Inst.*, vol. 349, no. 2, pp. 719–739, 2012.
[14] T. Madani and A. Benallegue, "Backstepping sliding mode control applied to a miniature quadrotor flying robot," in *Proc. Ind. Electron. Conf. (IECON)*, Nov. 2006, pp. 700–705.
[15] A. Das, F. Lewis, and K. Subbarao, "Backstepping approach for controlling a quadrotor using lagrange form dynamics," *J. Intell. Robot. Syst. Theory Appl.*, vol. 56, nos. 1–2, pp. 127–151, 2009.
[16] M. Huang, B. Xian, C. Diao, K. Yang, and Y. Feng, "Adaptive tracking control of underactuated quadrotor unmanned aerial vehicles via backstepping," in *Proc. Amer. Control Conf.*, Jun./Jul. 2010, pp. 2076–2081.
[17] J. Colorado, A. Barrientos, A. Martinez, B. Lafaverges, and J. Valente, "Mini-quadrotor attitude control based on Hybrid Backstepping & Frenet-Serret theory," in *Proc. IEEE Int. Conf. Robot. Automat. (ICRA)*, May 2010, pp. 1–6.
[18] C. Ha, Z. Zuo, F. B. Choi, and D. Lee, "Passivity-based adaptive backstepping control of quadrotor-type UAVs," *Robot. Auton. Syst.*, vol. 62, no. 9, pp. 1305–1315, 2014.
[19] C. Peng *et al.*, "Variable structure and variable coefficient proportional-integral-derivative control to prevent actuator saturation of yaw movement for a coaxial eight-rotor unmanned aerial vehicle," *Proc. Inst. Mech. Eng., G, J. Aerosp. Eng.*, vol. 229, no. 9, pp. 1661–1674, 2015.
[20] M. Saied, B. Lussier, I. Fantoni, C. Francis, and H. Shraim, "Fault tolerant control for multiple successive failures in an octorotor: Architecture and experiments," in *Proc. IEEE/RSJ Int. Conf. Intell. Robots Syst.*, Sep./Oct. 2015, pp. 40–45.
[21] M. Saied, B. Lussier, I. Fantoni, C. Francis, H. Shraim, and G. Sanahuja, "Fault diagnosis and fault-tolerant control strategy for rotor failure in an octorotor," in *Proc. IEEE Int. Conf. Robot. Automat. (ICRA)*, May 2015, pp. 5266–5271.
[22] M. Saied, H. Shraim, C. Francis, I. Fantoni, and B. Lussier, "Actuator fault diagnosis in an octorotor UAV using sliding modes technique: Theory and experimentation," in *Proc. Eur. Control Conf. (ECC)*, Jul. 2015, pp. 1639–1644.

RASHID ALI received the B.S. degree in electronics and telecommunication, in 2013, and the master's degree in signal and information processing from Northwestern Polytechnical University, Xi'an, China, in 2015. He is currently pursuing the Ph.D. degree with the School of Computer and Communication Engineering, University of Science and Technology Beijing, Beijing, China. He has published one book in Lambert Academic Publishing, Germany. He has several publications in international journals and international conference indexed by EI. His research interests include image processing, image denoising, image enhancement, image compression, and control systems. He was a recipient of the Chinese Government Scholarship (CSC).

PENG YUNFENG (M'11) received the B.E. degree from the Nanjing University of Science and Technology, in 1996, and the M.S. degree from the Kunming University of Science and Technology, in 2003, and the Ph.D. degree from Shanghai Jiaotong University, in 2007. He is currently a full time Professor with the Department of Communication and Information Engineering, University of Science and Technology Beijing, Beijing, China. His research interests include image processing and network communications.

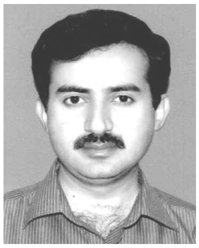

M. TOUSEEF IQBAL received the B.Sc. degree in electrical engineering from the University of Engineering and Technology, Taxila, Pakistan, in 2002, and the M.S. degree in system engineering from PIEAS, in 2005. He is currently with the Department of Electrical Engineering, University of Engineering and Technology, Taxila. His research interests include autonomous systems, control systems, and industrial automation.

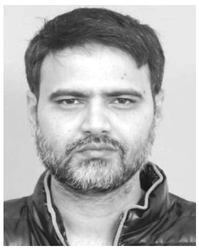

ROOH UL AMIN received the B.E. degree in industrial electronics from NED UET, in 2003, the M.S. degree in system engineering from PIEAS, in 2005, and the Ph.D. degree in control engineering from Northwestern Polytechnical University, Xi'an, China, in 2017, where he is currently a Senior Researcher with the School of Automation and Control. He has several publications in international journals and conferences and ISI, and Scopus indexed journals. His research interests include control engineering, intelligent systems, stochastic processes, and image processing. He is a Reviewer of several international journals and international conference.

M. OMER ZAHID received the B.Sc. degree in electrical engineering from the University of Engineering and Technology, Lahore, Pakistan, in 2011. He is currently pursuing the M.S. degree with the School of Mechanical and Manufacturing Engineering, National University of Science and Technology, Islamabad, Pakistan. His research interests include control systems of parallel and serial manipulators, motion control, and industrial automation.

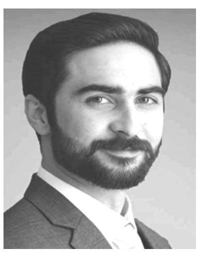

OMAIR IRFAN KHAN received the B.Sc. degree in electrical engineering from the University of Engineering and Technology, Taxila, Pakistan, in 2014, and the master's degree in project management from SZABIST University Islamabad, Pakistan, in 2017. He is currently pursuing the M.S. degree in robotics and intelligent machine engineering with the School of Mechanical and Manufacturing Engineering, National University of Science and Technology, Islamabad. His research interests include autonomous systems, control systems, and wireless communication.